He^3- and He^4-Induced Coulomb Excitation

D. A. BROMLEY, J. A. KUEHNER, AND E. ALMQVIST
Atomic Energy of Canada Limited, Chalk River, Ontario, Canada
(Received March 2, 1959)

In order to examine the characteristics of the He^3-induced Coulomb excitation process and the validity of the cross-section ratio technique for the identification of both $E1$ and $E2$ transitions, thick-target radiation yield ratios have been measured for He^3- and He^4-induced Coulomb excitation of each of the 110- and 197-kev levels of F^{19}, the 446-kev level of Na^{23}, the 160-kev level of Ti^{47}, and the 126-kev level of Mn^{55} at corresponding (equal ξ) energies. For the $E2$ transitions a mean ratio of the He^3- to He^4-induced yields of 0.63 ± 0.02 was found, independent of incident energy in the range 1.0 to 2.5 Mev, in agreement with the calculated value of 0.64 for F^{19} and Na^{23} and of 0.63 for Ti^{47} and Mn^{55}. In the single $E1$ transition (110 kev in F^{19}) studied, the experimental ratios range from 0.76 ± 0.07 at $E_{He^3}=1.00$ Mev to 0.59 ± 0.11 at $E_{He^3}=1.75$ Mev. While in accord with the theoretical prediction of 0.76 at the lower energies, the indicated energy dependence of the ratio is suggestive of contributions due to nuclear inelastic scattering of alpha particles. It has been demonstrated that the ratio technique, using He^3 and He^4 ions, provides an unambiguous multipolarity determination provided that inelastic-scattering contributions can be excluded.

INTRODUCTION

SINCE 1953 a very extensive body of information on the properties of low-lying nuclear levels has been obtained by using the Coulomb excitation process and detection of either the inelastically scattered charged particles or, more usually, the de-excitation gamma radiation from the states populated by Coulomb excitation. A complete treatment of the classical and quantum mechanical theory of this process together with a compilation of the available data and experimental techniques has been given in the excellent survey paper of Alder *et al.*[1] In almost every instance the measured quantities have been the excitation energy of the state in question and the reduced width for the transition; current collective models[2,3] have enjoyed remarkable success in correlating these data in terms of nuclear distortions and consequent enhanced intrinsic nuclear quadrupole moments. Of the several hundred states studied to date via Coulomb excitation, almost all have been shown to be populated via $E2$ transitions; in the de-excitation, in cases where $M1$ admixture is allowed by angular momentum considerations, the $M1$ component usually dominates the transition as in normal de-excitation studies. $M1$ Coulomb excitation is depressed in intensity by the usual $(v/c)^2$ factor, where v is the velocity of the incident particles, and is almost always completely negligible. Although the intrinsic $E1$ transition probability might be expected to be several orders of magnitude greater than the corresponding $E2$ value, the only case of an $E1$ transition amenable to study in light nuclei, as will be discussed later in detail, is that to the first excited state of F^{19}. The two reasons for this are the paucity of low-lying nuclear levels with parity opposite to that of the ground state at excitations $\leqslant 500$ kev (and thus accessible with the available incident energies) and the very low $E1$ matrix elements connecting these states. In general the $E1$ transition widths are 10^8 to 10^7 smaller than the single-particle estimates: from the shell model viewpoint in light nuclei this reflects the fact that essentially all these transitions involve at least one state of relatively complex character.[4] Since the $E1$ transition probability depends on a separation of the centroids of charge and mass, and since the effect of the electric field of the incident particle which induces this polarization is weak compared to the nuclear forces which favor a uniform charge distribution, it is intuitively reasonable that the observed transition probabilities are very much smaller than single-particle estimates. It is clear that the limitation on the number of $E1$ transitions studied reflects in part the limitations which have until recently restricted the bombarding particles to those of very low atomic number; this has effectively limited the nuclear excitations amenable to study to below several hundred kev. With the recent availability of heavy-ion beams in many laboratories[5] this effective limit has been moved up to $\sim$2.5 Mev[6] making practicable the study of the 1^- states at excitations $\sim$1 Mev in heavy even-even nuclei corresponding to the pear-shaped oscillations of the nuclear core.[7]

Particularly in the case of weak, low-energy transitions, correction for absorption of the emergent gamma radiation in the experimental equipment and in the target itself poses a difficult problem. In order to obtain cross sections, and thus the reduced transition widths, it is also necessary of course to measure the

[1] Alder, Bohr, Huus, Mottelson, and Winther, Revs. Modern Phys. **28**, 432 (1956).
[2] A. Bohr and B. R. Mottelson, Kgl. Danske Videnskab. Selskab, Mat.-fys. Medd. **27**, No. 16 (1953).
[3] S. G. Nilsson, Kgl. Danske Videnskab. Selskab, Mat.-fys. Medd. **29**, No. 16 (1955).
[4] M. Goldhaber and A. W. Sunyar, in *Beta- and Gamma-Ray Spectroscopy*, edited by K. Siegbahn (North-Holland Publishing Company, Amsterdam, 1955), Chap. XVI(II); S. G. Nilsson and J. O. Rasmussen, Nuclear Phys. **5**, 617 (1958).
[5] See Proceedings of the Conference on Reactions between Complex Nuclei, Gatlinburg, Tennessee, May 5–7, 1958, edited by Zucker, Livingston and Howard [Oak Ridge National Laboratory Report ORNL-2606, September, 1958 (unpublished)].
[6] J. O. Newton, in Proceedings of the Conference on Reactions between Complex Nuclei, Gatlinburg, Tennessee, May 5–7, 1958, edited by Zucker, Livingston, and Howard [Oak Ridge National Laboratory Report ORNL-2606 (unpublished)], Paper 25; and private communication.
[7] Stephens, Asaro, and Perlman, Phys. Rev. **100**, 1543 (1955).

effective target thickness, the incident flux, and the detector efficiencies. Bohr and Mottelson[8] suggested a method of determining the multipolarity of the transitions studied which is based only on the general features of the process and obviates the need for the aforementioned measurements. The method is based on the assumption that the contribution to the total transition width from the magnetic multipoles is negligible, as will be assumed throughout the discussion in this paper, and involves the determination of the ratio of the cross sections for Coulomb excitation of a particular nuclear level using two different bombarding particles at appropriately selected energies.[9]

For electric multipoles ($E\lambda$) the Coulomb excitation cross section may be written[1]

$$\sigma_{E\lambda}=\left(\frac{Z_1e}{\hbar v_i}\right)^2\left(\frac{Z_1Z_2e^2}{mv_iv_f}\right)^{-2\lambda+2}B(E\lambda)f_{E\lambda}(\xi), \quad (1)$$

where Z_1 and Z_2 are the atomic numbers of the incident and target nuclei, m is the reduced mass of the incident ion, v_i and v_f the relative velocities before and after collision, respectively, and λ the multipole order of the transition. $B(E\lambda)$ is the familiar reduced width and $f_{E\lambda}(\xi)$ is a relatively complex function of the radial matrix elements involved. The dimensionless argument ξ of this function is defined by

$$\xi=\eta_f-\eta_i, \quad (2)$$

where

$$\eta_{i,f}=Z_1Z_2e^2/\hbar v_{i,f}$$

is the Sommerfeld number before and after collision, respectively. Thus

$$\xi=\frac{Z_1Z_2e^2}{\hbar}\left\{\left(\frac{m}{2}\right)^{\frac{1}{2}}\frac{\sqrt{E_i}-\sqrt{E_f}}{\sqrt{(E_iE_f)}}\right\}, \quad (3)$$

where E_i and E_f are the projectile energies before and after collision, and for $E_f\rightarrow E_i$ (i.e., the excitation energy ΔE of the state involved negligible with respect to E_i) this reduces to the zero-energy approximation used in early studies in the field,[10]

$$\xi=(Z_1Z_2e^2/\hbar v)(\Delta E/2E). \quad (4)$$

It follows from Eq. (1) that if, in the method noted above, the two projectile energies are selected so that the two ξ parameters are equal, then the ratio of the Coulomb excitation cross sections is independent of both the $B(E\lambda)$ and $f_{E\lambda}(\xi)$ factors as well as being independent of the experimental parameters listed previously.

This technique was first applied by Bjerregaard and Huus[9] for $E2$ excitations by protons, deuterons, and alpha particles on wolfram and by Temmer and Heydenburg[11] for $E2$ excitations by protons and alpha particles on F^{19}, Mn^{55}, and Na^{23}. In the case of alpha and proton bombardment, the computed ratio is

$$\sigma_{CE}(\alpha)/\sigma_{CE}(p)\begin{matrix}\approx 6.4 \text{ for } E1 \text{ transitions}\\ \approx 10.1 \text{ for } E2 \text{ transitions,}\end{matrix}$$

and the measurements for all states were in reasonable agreement with the value of 10 expected for $E2$ transitions.[12] It should be noted that in principle the multipolarity of a transition may be obtained from the shape of the excitation curve alone; in general, however, this technique is not capable of making unambiguous assignments. In the case of the 110-kev state in F^{19}, for example, it was not possible to distinguish unambiguously between $\lambda=1$ and $\lambda=2$ using the excitation function data obtained by the above authors although the results of Sherr, Li, and Christy[13] do appear to decide unambiguously between these possibilities. Other data on the lifetime,[14] angular distribution,[15] and K-shell internal conversion coefficient[16] of the radiation do establish this as an $E1$ transition. The ratio technique was not applied because of difficulties experienced in resolving the 110-kev transition in bombardments with other than alpha particles.

Several difficulties are encountered in using protons and alpha particles as the two projectiles in this technique. The dipole bremsstrahlung cross section may be written[1] as

$$d\sigma_{E1}=1.225\times10^{-8}Z_1^2Z_2^2\left(\frac{Z_1}{A_1}-\frac{Z_2}{A_2}\right)^2\frac{A_1}{E}f_{E1}(\xi)\frac{dE_x}{E_x}, \quad (5)$$

where the notation is as above and E_x is the energy of the bremsstrahlung quantum. Because of the factor $(Z_1/A_1-Z_2/A_2)^2$ related to the separation of the charge and mass centroids in the collisions, protons are predicted theoretically, and found experimentally, to give an $E1$ bremsstrahlung yield a factor of from 10^2 to 10^4 greater than alpha particles on the same target nucleus. Thus in proton bombardment low-energy Coulomb excitation lines are frequently masked by the bremsstrahlung yield.

Only dipole bremsstrahlung has been considered here since the relative intensity of consecutive multipole orders is $\sim\{\xi(v/c)\}^2$; magnetic multipoles are similarly reduced in intensity relative to the corresponding electric ones by a factor $\{v/c\}^2$. It should be noted however that since the dipole bremsstrahlung vanishes for alpha-particle bombardment of a self-conjugate target and is small for all light targets where $A\approx2Z$,

[8] A. Bohr and B. R. Mottelson, as quoted by J. H. Bjerregaard and T. Huus, Phys. Rev. **94**, 204 (1954).
[9] J. H. Bjerregaard and T. Huus, reference 8.
[10] C. Zupančič and T. Huus, Phys. Rev. **94**, 205 (1954).
[11] G. M. Temmer and N. P. Heydenburg, Phys. Rev. **96**, 426 (1954).
[12] N. P. Heydenburg and G. M. Temmer, *Annual Review of Nuclear Science* (Annual Reviews, Inc., Palo Alto, 1956), Vol. 6, p. 77; Phys. Rev. **100**, 150 (1955).
[13] Sherr, Li, and Christy, Phys. Rev. **96**, 1258 (1954), and Phys. Rev. **94**, 1076 (1954).
[14] Thirion, Barnes, and Lauritsen, Phys. Rev. **94**, 1076 (1954).
[15] R. F. Christy, Phys. Rev. **94**, 1077 (1954).
[16] Mills, Hilton, and Barnes (to be published).

the residual bremsstrahlung yield has in general electric quadrupole and magnetic dipole components.[1]

Furthermore, because of the lower Coulomb barrier, inelastic scattering processes compete with Coulomb excitation at much lower incident energies for protons than for alpha particles and make interpretation of the ratio data uncertain to the extent that these competing processes cannot be excluded. Finally, at energies corresponding to equal ξ values, i.e., $E_\alpha \sim 2.5E_p$, the particle ranges are significantly different and a correction must be applied for this if targets of appreciable thickness are to be employed. For these reasons the ratio technique has not been applied previously to a dipole transition. Since the range-energy relationship for alpha particles and the relationship between proton and alpha-particle ranges used in the above experiments are not at all well known for low energies, ratio measurements have been restricted to thin targets.

It is clear from the foregoing that He^3 and He^4 ions have considerable advantages as the two projectiles in ratio measurements. Bremsstrahlung yield from He^3 bombardments, while greater by ~ 50 than from He^4 bombardment, is less than in the corresponding proton case by a factor $\sim 10-100$. The Coulomb barriers are roughly equal for He^3 and He^4; because of the high He^3 mass excess, the number of open channels in He^3-induced reactions usually far exceeds that in He^4-induced ones[17] and as a consequence, inelastic scattering contributions should be less pronounced in He^3 than in He^4 reactions. Finally the He^3 and He^4 ranges are directly related,[18] i.e.,

$$R_{He^3}(E) = aR_{He^4}(E/a), \quad \text{where} \quad a = M_{He^3}/M_{He^4}, \tag{6}$$

and the range corrections are simply computed for thick target bombardment in all materials. The major difference, as compared to proton-alpha measurements, is that because of the smaller difference between the masses and the equal charges of the incident particles, the predicted ratio is much closer to unity. The quantity of interest in a determination of the transition multipolarity is not the absolute value of the ratio but rather the difference in the ratio values for different multipoles. As an example, in the case of the 197-kev transition in F^{19}, the calculated cross-section ratio for an $E2$ transition is 1.7 times that for an $E1$ for p and α excitation whereas for He^3 and He^4 excitation the calculated $E1$ ratio is 1.2 times the corresponding $E2$ ratio.

The measurements to be reported herein using He^3 and He^4 ions as incident particles were carried out to verify the validity of the ratio technique for $E2$ transitions; to examine its applicability to a dipole transition using these two projectiles; and to examine the characteristics of He^3-induced Coulomb excitation which have not been reported previously in the literature. Transitions of known multipolarity were selected in convenient target nuclides; for $E2$ transitions these included F^{19} (197 kev), Na^{23} (446 kev), Ti^{47} (160 kev), and Mn^{55} (126 kev), and for $E1$ transitions the single example is that of 110 kev in F^{19}.

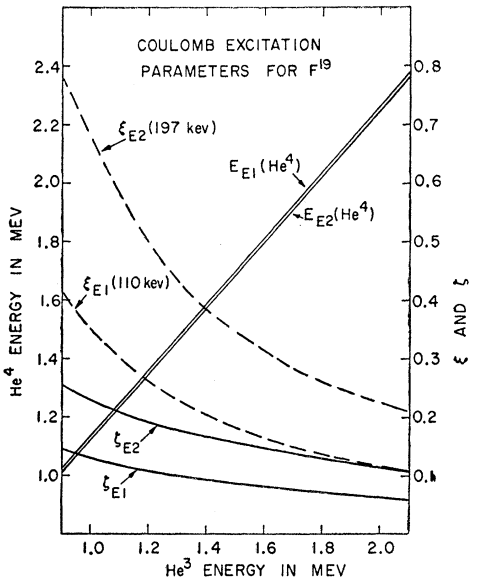

FIG. 1. Parameters relating to Coulomb excitation studies on F^{19} as defined by Eqs. (8), (11), and (12) in the text for incident He^3 and He^4 ions.

SELECTION OF CORRESPONDING ENERGIES

Defining ΔE, m_T, m_j, E_j as the excitation of the nuclear state in question, the target nuclear mass, the projectile mass, and the projectile incident energy, respectively, where j represents He^3 or He^4 ions, the quantities of interest are[1]

$$\Delta E_j' = (1+m_j/m_T)\Delta E, \tag{7}$$

$$\zeta_j = \Delta E_j'/E_j, \tag{8}$$

$$(\eta_i)_j = \tfrac{1}{2}Z_jZ_T\left\{\frac{m_j}{10.084E_j}\right\}^{\frac{1}{2}}, \tag{9}$$

$$(\eta_f)_j = (\eta_i)_j/(1-\zeta_j)^{\frac{1}{2}}, \tag{10}$$

$$\xi_j = (\eta_f)_j - (\eta_i)_j, \tag{11}$$

$$= \tfrac{1}{2}Z_jZ_T\left\{\frac{m_j}{10.084E_j}\right\}^{\frac{1}{2}} \times\left\{\left[1-\left(1+\frac{m_j}{m_T}\right)\frac{\Delta E}{E_j}\right]^{-\frac{1}{2}}-1\right\}. \tag{12}$$

Having selected convenient incident energies for the

[17] D. A. Bromley and A. R. Rutledge, Chalk River Report CRP-789, September, 1958 (unpublished).

[18] H. Bethe and J. Ashkin, in *Experimental Nuclear Physics*, edited by E. Segrè (John Wiley & Sons, Inc., New York, 1953), Vol. 1.

He^3 ions, the corresponding (i.e., equal-ξ) values of alpha energies were obtained by solving Eq. (12) numerically. In some cases the measurements were initially carried out at corresponding energies given by the zero-energy approximation of Eq. (4); the final data are corrected however to correspond to Eq. (12). Table I lists the energies used for F^{19} (197-kev state) and illustrates the error involved in using the zero-energy approximation. Figure 1 shows the relevant parameters for F^{19} as functions of the incident He^3 energy. Table II lists the energies used with the Na^{23}, Ti^{47}, and Mn^{55} targets.

EQUIPMENT

In these ratio measurements a 40/60 mixture of He^3 and He^4 gas was supplied to the ion source of the Chalk River 3-Mev accelerator in order to facilitate the transfer between the two ion beams without changes in the system other than in the magnetic field of the 90° analyzer magnet. Following the 90° analyzer a single magnetic quadrupole lens unit was used to correct the astigmatic focus of the analyzer and give a sharply defined target spot. A simple Lucite adaptor was provided for the standard target assemblies in use[19] which permitted the installation of extensive shielding around the target and detector volume and interposed only $\frac{1}{16}$ in. Lucite between the target and detector. Figure 2 is a schematic drawing of this assembly as used in some of the early measurements. In a later version, the beam path between the aperture block and the target was extended to allow for the construction of a 2-in. thick lead enclosure with at least 7 in. separation between its inner surface and the target and detector system. Gamma radiation was detected at 90° to the incident beam in either a $1\frac{1}{4}$-in.$\times$1-in. or $1\frac{1}{2}$-in.$\times$2-in. NaI(Tl) crystal optically coupled to an RCA 6655 photomultiplier. The angular acceptance was $\sim$100°. Output pulses were delay-line shaped, amplified, and displayed on a 100-channel Goulding transistorized pulse-height analyzer.[20]

TABLE I. Corresponding He^3 and He^4 energies for equal ξ values for Coulomb excitation of the 197-kev state in F^{19}. E_{He^4} is the exact classical result [Eq. (12)] whereas $E_{He^4}{}^*$ is the zero-energy approximation [Eq. (4)].

EHe^3 Mev	ξ	EHe^4 Mev	EHe^{4*} Mev
	F^{19} (197-kev state)		
1.00	0.681	1.120	1.132
1.20	0.500	1.347	1.358
1.40	0.387	1.574	1.585
1.75	0.269	1.970	1.981
2.00	0.225	2.254	2.264

[19] Bromley, Gove, Kuehner, Litherland, and Almqvist, Phys. Rev. **114**, 758 (1959).

[20] F. H. Goulding, Natl. Acad. Sci.—Natl. Research Council, Publ. No. 467, 86 (1956).

TABLE II. Corresponding He^3 and He^4 energies for equal ξ. See caption of Table I.

EHe^3 Mev	ξ	EHe^4 Mev	EHe^{4*} Mev
	Na^{23} (446-kev state)		
2.0	0.653	2.229	2.253
	Ti^{47} (160-kev state)		
1.40	0.681	1.550	1.558
1.75	0.477	1.940	1.948
2.00	0.387	2.218	2.226
	Mn^{55} (126-kev state)		
1.40	0.591	1.550	1.555
1.75	1.416	1.938	1.944
2.00	0.338	2.216	2.222

Thick targets of NbF_5 were prepared by evaporating concentrated hydrofluoric acid on niobium blanks. The fluoride layer thus prepared was quite stable under lengthy bombardment with ion beams of several microamperes in the 1- to 3-Mev range. Niobium was used as a target backing because it has no Coulomb-excitation gamma radiation or characteristic x-radiation in the energy range of interest (40 to 300 kev) and has a sufficiently high Coulomb barrier to inhibit effectively competition from other nuclear reactions at the He ion energies in use. Thick targets of fused sodium chloride on tantalum backings and of metallic titanium and manganese were also used. The chlorine isotopes present in the NaCl target contribute no background interference at the bombarding energies used. The first excited states in Cl^{35} and Cl^{37} are at 1.220 and 1.72

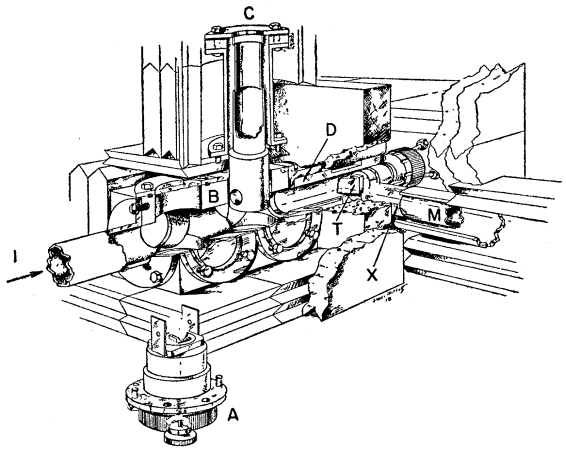

FIG. 2. Schematic representation of the experimental equipment. The incident ion beam I after traversing the 90° analyzer and quadrupole focusing magnets passed through a standard block B containing a liquid nitrogen trap C and a retractable quartz viewer and aperture block A. The Lucite assembly D carried a standard oil-cooled 45° target mount T; $1\frac{1}{2}$-in.$\times$2-in. or $1\frac{1}{4}$-in.$\times$1-in. NaI(Tl) crystals X optically coupled to an RCA 6655 2-in. photomultiplier M were completely shielded from the laboratory and beam plumbing by lead and heavy concrete brick walls. As noted in the text, in the F^{19} measurements the shield walls were moved away from the target and detector to minimize the back-scatter contribution.

Mev, respectively,[21] precluding their excitation by the Coulomb process at the incident energies used; the higher Coulomb barrier prevents appreciable yield of He-induced nuclear reaction contaminants from the chlorine isotopes.

In heavy-element bombardment it was found convenient to surround the target chamber with a 0.015-in. cadmium absorber to preferentially remove the low-energy bremsstrahlung and x-radiation; the K-absorption edge for cadmium is at 26.71 kev.

Calibration sources of Am^{241} (60 kev), Lu^{177} (115 and 208 kev), Ce^{141} (142 kev), Hg^{203} (279 kev), Cr^{51} (322 kev), Au^{198} (412 kev), and Na^{22} (511 kev) were used to establish the detector energy calibration and the standard spectral shapes in the detector and shielding geometry in use.

In order to examine the gamma-radiation yields in the energy range $\sim 50-500$ kev it was found necessary to install as complete shielding as possible about the detector. This was particularly the case during these measurements because of the copious yield of gamma radiation from He^3 bombardment of the surface contaminants such as carbon in the system. Even with the He^4 beam analyzed and on target, the He^3 component which was intercepted by the magnet vacuum system produced a high background in the experimental area.

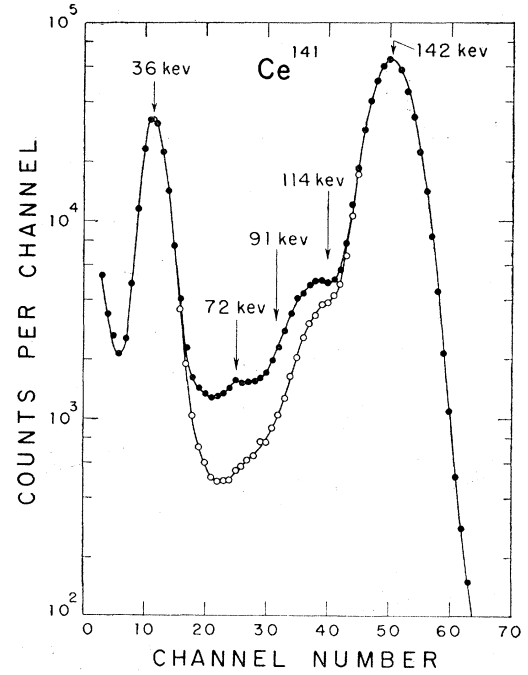

FIG. 3. Gamma radiation spectra from a Ce^{141} source mounted in the target geometry. Curve A was obtained in the large shield enclosure; curve B was measured with all shielding material removed, while curves C and D were obtained in the enclosure with lead and iron scatterers mounted on the opposite side of the source to the detector. The 1-μC Ce^{141} source was deposited on a 0.010-in. niobium blank.

[21] P. M. Endt and C. M. Braams, Revs. Modern Phys. **29**, 683 (1957).

The energy scale of the analyzer magnet was calibrated by examining the $B^{10}(\alpha,p\gamma)C^{13}$ reaction in the region of the 1.518-Mev resonance using the target and detector system described above.

RESULTS

Spectral Shapes

In order to obtain standard spectral shapes for use in the analysis of the Coulomb excitation spectra, a series of measurements was carried out using the sources listed in the previous section. These measurements were particularly important for the F^{19} studies since the energy of the back-scattered Compton quanta associated with the 197-kev transition is 110 kev. Because the dipole transition in F^{19} is of precisely this energy it was necessary to make an experimental determination of the contribution to the apparent yield of 110-kev radiation resulting from this back-scattering from the target backing and environment.

Figure 3 illustrates the results of a series of measurements carried out with a 1-μC source of Ce^{141} deposited on an 0.010-in. Nb backing identical to that used for the NbF_5 targets. All runs were of equal duration thus automatically normalizing the 142-kev peak and that at 36 kev corresponding to the K x-ray of the Pr^{141} daughter populated in the Ce^{141} decay.

Curve C was obtained with the source in the target geometry but with Pb shielding $\sim\frac{1}{2}$ in. away from it and shows the characteristic Pb K x-ray of 72 kev.[22] The yield of back-scattered Compton quanta which have a lower energy limit of 91 kev for this source is not significantly higher than that shown in curves A or B which correspond, respectively, to measurements carried out with the Pb shielding removed to $\geqslant 7$ in. from the source and detector and with the shielding completely removed from the source vicinity. Time-dependent backgrounds obtained from identical no-source runs have been subtracted from the data presented. The absence of back-scattered quanta from Pb at this energy (91 kev)[23] is not unexpected since the critical K x-ray absorption edge is at 87.95 kev.[22] Curve A, measured in the expanded shielding geometry, shows clearly the residual yield of Pb x-radiation. Curve D was obtained by placing a $\frac{1}{4}$-in. Fe plate $\sim\frac{1}{2}$ in. from the source opposite to the detector and shows the characteristic back-scattered radiation. This enhancement of the back-scatter from iron as opposed to lead results from the fact that the ratio of scattering to absorption cross sections for iron is 48 and 35 times that for lead at 200 and 100 kev, respectively.[24] The

[22] J. M. Cork, in *Handbook of Chemistry and Physics* (Chemical Rubber Publishing Company, Cleveland, Ohio, 1956–57), thirty-eighth edition, p. 2437.

[23] Anne T. Nelms, National Bureau of Standards, Circular No. 542, August, 1953 (U. S. Government Printing Office, Washington, D. C., 1953).

[24] Storm, Gilbert, and Israel, Atomic Energy Commission Report TID-4500, 1958 (unpublished), thirteenth edition revised.

escape of the iodine K x-ray of 28.2 kev from the crystal results in the low-energy shoulder on the total absorption peak.

From the difference between curves A and B and the shape of the back-scatter yield as obtained from the difference between curves D and A, the back-scatter yield from the large Pb shield enclosure was found to be $0.3\pm0.3\%$ of the total absorption peak at 142 kev.

Since the ratio of scattering to absorption cross sections for Nb are $\sim$10 and 7.5 times those for Pb at 200 and 100 kev, the 0.010-in. target and source backings were expected to produce appreciable back-scattering. In order to obtain the magnitude of this effect the measurements shown in Figs. 4 and 5 were

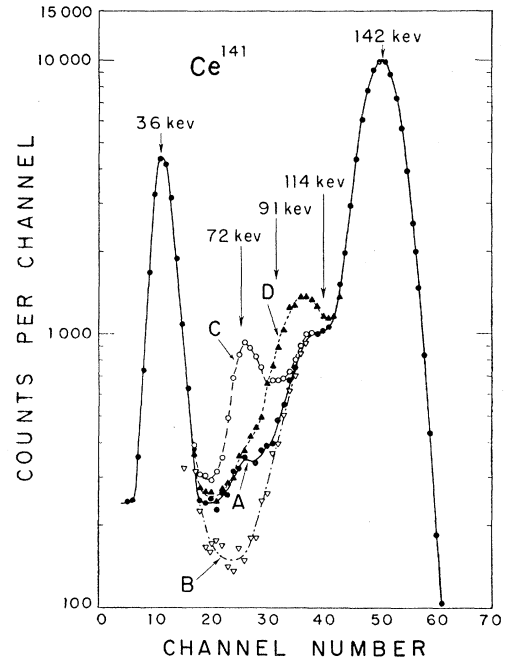

FIG. 4. Gamma radiation from a Ce^{141} source deposited on 0.0005-in. Mylar. The closed circles represent data obtained with an 0.010-in. niobium blank immediately behind the source in the large shield enclosure; the open circles represent data obtained with both shielding and the niobium blank removed.

carried out with 1-μC sources of Ce^{141} and Cr^{51} deposited on 0.0005-in. Mylar film. These sources were selected since they bracket the 197-kev energy from F^{19} and give isolated gamma-radiation lines amenable to detailed spectral analysis. In these figures the closed circles represent data obtained with the sources in the target geometry, with the large shield enclosure and with a 0.010-in. Nb blank against the Mylar source backing immediately opposite the detector. The open circles represent data obtained with identical source and detector geometry but with all shielding and the Nb blank removed. Background corrections have been included wherever significant. From the differences between the two curves back-scatter contributions of

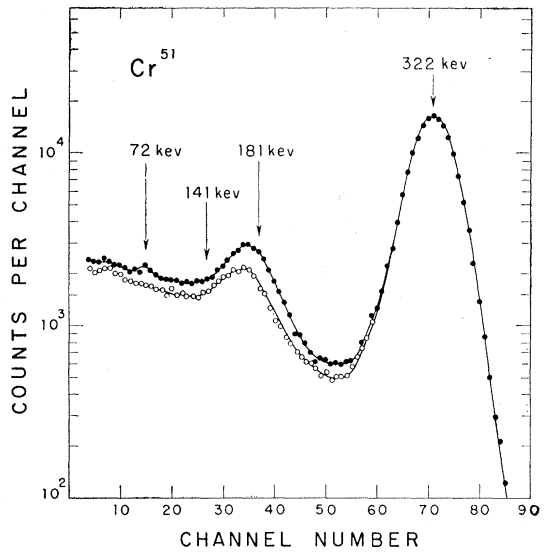

FIG. 5. Gamma radiation from a Cr^{51} source deposited on 0.0005-in. Mylar. See caption to Fig. 4.

(2.6 ± 0.3) and (5.0 ± 0.5) percent of the total absorption peaks were measured for the 142- and 322-kev lines, respectively. These figures include the effects of both the 0.010-in. Nb backings and of the shield enclosure The residual yields of 72-kev Pb x-rays are shown in both figures; the Compton edges are at 50 and 181 kev. respectively.[23]

From these back-scattering data, that for the 197-kev radiation from F^{19} is obtained by linear interpolation as 3.3% and a standard deviation of 0.6% has been assigned to include uncertainty regarding the validity of this interpolation.

All data presented in Figs. 3, 4, and 5 were obtained using a $1\frac{1}{4}$-in.$\times$1-in. NaI(Tl) crystal. The back-scatter contribution of 3.3% obtained here is significantly lower than the value $\sim$9% obtained by Lindqvist and Wu[25] in this energy region; this higher value was measured, however, under appreciably different geometric conditions.

F^{19} Results

Figures 6 and 7 show typical spectra obtained by bombarding NbF_5 targets with both He^3 and He^4 ion beams. The inset level diagram in Fig. 6 shows the transitions involved in F^{19}. These spectra correspond to equal charge delivered to the target. The indicated energies of 169 and 82 kev correspond to the expected positions of the iodine x-ray escape peaks; 72 and 17 kev are the energies of the K x-rays from the lead shielding and the niobium target backings, respectively. For an incident He^3 energy of 1.00 Mev there is essentially no yield of higher gamma radiation from the NbF_5 target; at 1.75 Mev, as shown in Fig. 7, there is an appreciable background resulting from the tails of

[25] T. Lindqvist and C. S. Wu, Phys. Rev. **100**, 145 (1955).

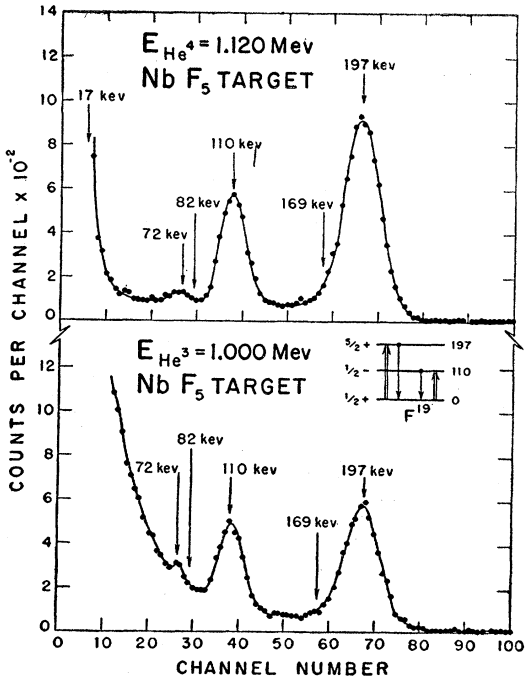

FIG. 6. Gamma radiation spectra from Coulomb excitation of F^{19}. The inset level diagram indicates the transitions observed. The backing spectra from niobium were measured with the same total beam charge on target as on the NbF_5 targets.

higher-energy reaction gamma radiation. Measurements with a Nb target demonstrate that there is no reaction or Coulomb-excitation gamma radiation from the Nb component of the NbF_5 targets; there is however an intense 17-kev K x-ray and, particularly in the case of incident He^3 ions, appreciable bremsstrahlung radiation.

As illustrated in Fig. 7, experimental difficulties peculiar to F^{19} made it unfeasible to extend the ratio measurements to He^3 energies higher than 1.75 Mev. Because of the much more rapid increase in the $E2$ Coulomb excitation cross section populating the 197-kev state than in the $E1$ cross section to the 110-kev state, with increasing incident energy and the increasing reaction background, the accuracy with which the 110-kev radiation yield from the corresponding state can be separated from the larger back-scatter contributions at this energy from the 197-kev radiation and from the reaction and bremsstrahlung background decreases rapidly. This is reflected directly as a larger uncertainty in the observed He^3 to He^4 yield ratio. Spectra obtained at higher energies did not permit extraction of the yield ratio with sufficient accuracy to allow significant comparison with theoretical predictions.

Ratio measurements similar to those shown in Figs. 6 and 7 have been carried out at He^3 energies of 1.20 and 1.40 Mev and at the corresponding He^4 energies as listed in Table I.

Comparison of Fig. 6 showing the spectrum measured with alpha-particle bombardment of F^{19} with that of Fig. 1 of Jones and Wilkinson[26] taken at lower resolution confirms these authors' supposition that the step observed on the lower edge of their 110-kev peak was due to x-radiation from the shielding. There is no evidence for any $M2$ cascade radiation of 87 kev from the 197-kev level via that at 110 kev. An experimental upper limit of 1% of the direct 197-kev transition follows from the measurements reported herein. The extreme Weisskopf[27] single-particle model would predict a branching ratio of 0.3×10^{-4} in accord with this limit.

The level assignments in these and subsequent figures are taken from the appropriate nuclear data compilations.[21,28,29]

Na^{23} Results

Figure 8 shows the results of similar measurements carried out on a target prepared by fusing a thick layer of NaCl on a tantalum backing. This figure illustrates clearly the major difficulty experienced in studying He^3-induced Coulomb excitation in this region of excitation. Because of its high charge-to-mass ratio and high mass excess (15.814 Mev), He^3-induced reactions leading to positron emitters occur with high

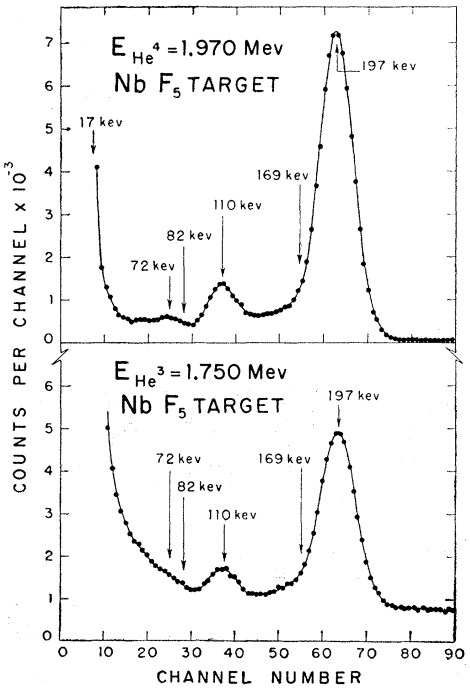

FIG. 7. Gamma radiation spectra from Coulomb excitation of F^{19}. See caption to Fig. 4.

[26] G. A. Jones and D. A. Wilkinson, Phil. Mag. **45**, 230 (1954).
[27] D. H. Wilkinson, Atomic Energy Research Establishment Report AERE T/R 2492, Harwell, 1958 (unpublished).
[28] F. Ajzenberg and T. Lauritsen, Revs. Modern Phys. **27**, 77 (1955).
[29] *Nuclear Data Sheets*, edited by C. L. McGinnis *et al.* (National Research Council, Washington, D. C.).

probability[17,30] and the resulting 0.511-Mev annihilation quanta obscure this energy range in the gamma-ray spectra. In bombardment of Na^{23}, for example, the positron emitters formed are $Al^{25}[Na^{23}(He^3,n)Al^{25}]$, $Na^{22}[Na^{23}(He^3,\alpha)Na^{22}]$ as well as $O^{14}[C^{12}(He^3,n)O^{14}]$ from the usual carbon contaminant layer on the target. These activities have half-lives of 7.62 ± 0.13 sec, 2.58 ± 0.03 years,[21] and 72.1 ± 0.4 sec,[28] respectively. The individual He^3 bombardments were limited to $\sim$1-min duration followed by a waiting period to allow the decay of the activity produced; this was found to give minimal background effects. Although this technique reduced the yield of 0.511-Mev radiation, as shown in the figure it was not possible to obtain as accurate intensity measurements on the Coulomb excitation gamma radiation as in the case of other targets with gamma energies further removed from the 0.511-Mev region.

At He^3 energies above 2.0 Mev the yield of 0.511-Mev radiation rose rapidly with incident energy and precluded the possibility of further ratio measurements.

Ti^{47} Results

Figure 9 presents typical spectra measured using a metallic foil of titanium 0.002 in. thick as target. In normal titanium the isotopes of mass 46, 47, 48, 49, and 50 have percentage abundances of 7.95, 7.75, 73.45, 5.51, and 5.34, respectively.[31] The lowest excited states in these nuclides are at 0.885, 0.160, 0.986, 1.38, and 1.595 Mev, respectively,[29] and as a result, at the energies used in these measurements only the 160-kev level in Ti^{47} is appreciably excited obviating the need for separated isotopic targets. In He^4 bombardments the background yield under the 160-kev peak was quite negligible; in He^3 bombardments the dv/v tail of the bremsstrahlung spectrum extends up to and beyond this region with appreciable yield. This figure provides an excellent illustration of the relative bremsstrahlung yield resulting from He^3 and He^4 incident ions; this yield completely masks the lead x-ray in the former case but not in the latter as shown in the upper spectrum in the figure. Ratio measurements have been made at He^3 energies of 1.40 and 2.00 Mev.

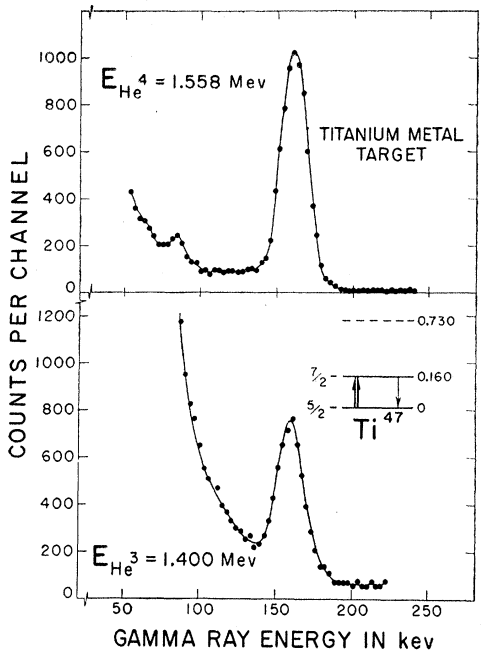

FIG. 9. Gamma radiation spectra from Coulomb excitation of Ti^{47}. The inset level diagram shows the transition observed. This figure clearly illustrates the higher bremsstrahlung production in He^3 as compared to He^4 bombardments.

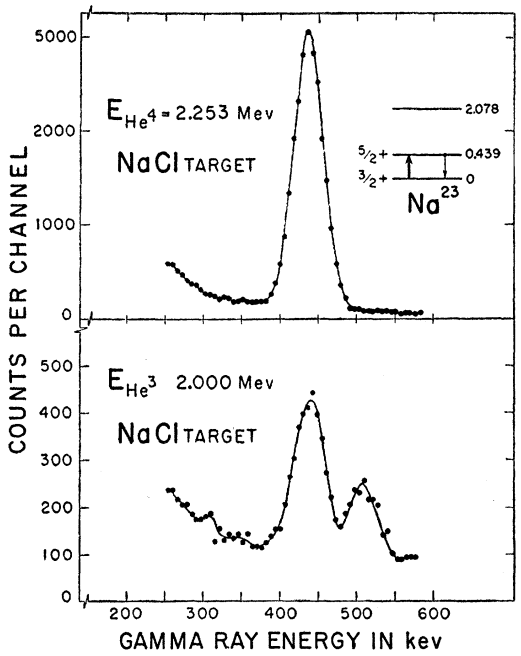

FIG. 8. Gamma radiation spectra from Coulomb excitation of Na^{23}. The inset level diagram indicates the transition observed. The second peak in the lower figure corresponds to the ubiquitous 0.511-Mev annihilation radiation from He^3-induced reactions.

Mn^{55} Results

Figure 10 shows the result of similar measurements on a 0.010-in. manganese metallic foil. Since magnanese is monoisotopic this transition is uniquely assigned to Mn^{55} as studied previously by many investigators using He^4 and protons. Ratio measurements have been made at He^3 energies of 1.40 and 2.0 Mev. In obtaining the spectra shown in this figure a thin cadmium absorber was interposed between the target and detector to reduce the bremsstrahlung intensity at the detector.

[30] D. A. Bromley and E. Almqvist, *Reports on Progress in Physics* (to be published).

[31] Sharp, Kennedy, Sears, and Hoyle, Chalk River Report CRT-556, 1954 (unpublished).

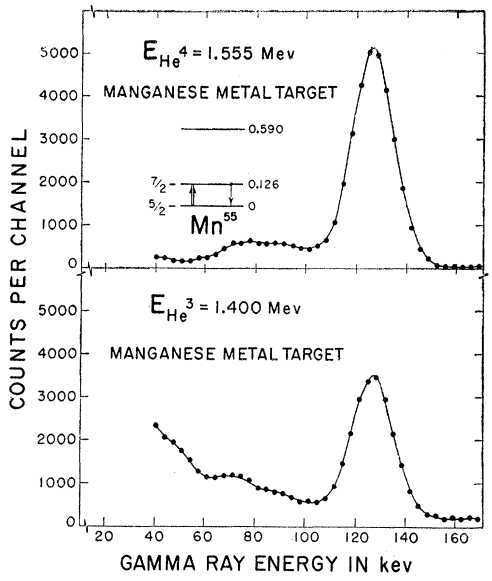

FIG. 10. Gamma radiation spectra from Coulomb excitation of Mn^{55}. The inset level diagram shows the observed transition. A cadmium absorber has been used to reduce the yield of low-energy bremsstrahlung radiation.

The measurements reported on Ti^{47}, Mn^{55}, and Na^{23} were carried out using a $1\frac{1}{2}$-in.$\times$2-in. NaI(Tl) detector in the smaller shielding enclosure described previously. This system gave somewhat higher efficiency and better shielding albeit with increased back-scatter. Relative measurements on these targets are not affected by this back-scatter in contrast to those on F^{19}.

Figures 6–10 show the results of single runs taken at the indicated energies and using the indicated targets. Both in order to obtain better statistical accuracy and to check on the target conditions, repeated He^4 and He^3 measurements were alternated with waiting periods following the He^3 measurements to allow the positron activities produced to decay. With the targets used, the spectra were accurately reproduced in repeated measurements demonstrating the target stability.

Extraction of Radiation Yields

Extraction of the radiation yields from spectra such as those illustrated in the above figures presented no difficulties in the cases of the Ti^{47} and Mn^{55} targets where only isolated peaks were involved as in the case of the 197-kev transition in F^{19}. In each of these cases the contribution from time-dependent and reaction backgrounds was subtracted directly. For He^4 bombardments this background contribution was quite negligible; the higher reaction yield corresponding to He^3 bombardment and the higher He^3 bremsstrahlung yield result in an uncertainty in this subtraction which is reflected by the quoted standard deviations in Tables III and IV.

In the case of the Na^{23} target the 0.511-Mev contribution in the region of the 439-kev peak was determined by fitting a standard 0.511-Mev spectral shape as obtained with a Na^{22} source to the experimental spectra. The additional uncertainty associated with this fitting is reflected in the larger standard deviation quoted in Table IV.

As noted previously, the problems of background subtraction were particularly marked in the case of the 110-kev transition in F^{19} induced by He^3 bombardment. This background included contributions from the normal tail of the 197-kev spectrum, from the Compton back-scatter of this radiation, from the $(d\nu/\nu)$ bremsstrahlung spectrum, from the higher-energy reaction gamma radiation, as well as from the very small environmental background.

In extracting the 110-kev radiation yield from the He^3 measurements, the 110-kev peak shape as observed in the He^4 data was used as a standard. By subtracting this fitted shape from the He^3 data, previously corrected for higher-energy reaction radiation and environmental background, the shape of the composite bremsstrahlung spectrum from both Nb and F^{19} was obtained. This shape was smoothed and in turn subtracted from the original spectrum, less background as noted, to give a 110-kev yield. This yield, and that obtained directly from the He^4 data, were then corrected for the $(3.3\pm0.6)\%$ back-scatter contribution from the 197-kev radiation. In all instances, the purely statistical errors in the yields were less than 1%. The major uncertainty as reflected by the quoted standard deviations in Table III is that in the shape of the extracted bremsstrahlung and background spectra in the region of 110 kev.

A cursory inspection of Eq. (5) for the $E1$ bremsstrahlung cross section suggests that the relative bremsstrahlung yields from Nb and F should be roughly in the ratio of $(41/9)^2\sim21$. Detailed evaluation of this expression shows however that for thin targets and 1.00-Mev incident He^3 ions for example, the relative cross sections for the production of 110-kev bremsstrahlung radiation are in the ratio of ~0.4. In this example the $f_{E1}(\xi)$ are in the ratio of $\sim7.5\times10^{-3}$ and dominate the expression, reflecting the fact that the

TABLE III. Results of Coulomb excitation cross-section ratio measurements for He^3 and He^4 ions on F^{19}. E_γ is the transition energy, $(J\pi)_{i,e}$ the angular momentum assignments for initial and excited states, E_{He^3,He^4} is the bombarding energy, ξ the Coulomb excitation parameter, and R_E the cross-section ratio.

E_γ kev	$(J\pi)_i$	$(J\pi)_e$	E_{He^3}	E_{He^4}	ξ	$R_{E\lambda}$
110	$\frac{1}{2}^+$	$\frac{1}{2}^-$	1.000	1.127	0.347	0.76±0.07
			1.200	1.352	0.230	0.71±0.04
			1.400	1.578	0.203	0.72±0.13
			1.750	1.975	0.143	0.59±0.11
197	$\frac{1}{2}^+$	$\frac{5}{2}^+$	1.000	1.120	0.681	0.62±0.03
			1.200	1.347	0.500	0.61±0.02
			1.400	1.574	0.387	0.63±0.02
			1.750	1.970	0.269	0.61±0.02

TABLE IV. Results of Coulomb excitation cross-section ratio measurements for Na^{23}, Ti^{47}, and Mn^{55} targets and He^3 and He^4 incident ions. E_γ is the transition energy, $(J\pi)_{i,e}$ the angular momentum assignments for initial and excited states, E_{He^3,He^4} is the bombarding energy, ξ the Coulomb excitation parameter, and $R_{E\lambda}$ the cross-section ratio.

Target	E_γ kev	$(J\pi)_i$	$(J\pi)_e$	E_{He^3}	E_{He^4}	ξ	$R_{E\lambda}$
Na^{23}	439	$\frac{3}{2}+$	$\frac{5}{2}+$	2.00	2.229	0.653	0.55±0.10
Ti^{47}	160	$\frac{5}{2}+$	$\frac{7}{2}+$	1.40	1.550	0.681	0.65±0.03
				2.00	2.218	0.387	0.63±0.03
Mn^{55}	126	$\frac{5}{2}-$	$\frac{7}{2}-$	1.40	1.549	0.591	0.63±0.03
				2.00	2.216	0.338	0.62±0.03

He^3 ions approach closer to the F^{19} nucleus and produce a greater overlap of radial wave functions. The experimental observations confirm this calculation qualitatively in that the apparent thick-target bremsstrahlung yield from F at 110 kev is several times that from Nb.

DISCUSSION

Excitation Functions

The large body of experimental data on Coulomb excitation measurements with thin targets[1] has established, to rather high precision, the validity of the semiclassical predictions of excitation functions. The corrections which must be applied in the case of thick targets are in a somewhat less satisfactory condition.

Since absolute cross sections have not been measured in these experiments, in comparing the excitation functions obtained with the theoretical predictions it has been necessary to normalize the two; this normalization has been carried out at the lowest energies measured where competing contributions would be expected to be minimal. From Eq. (7) it follows that for $E1$ transitions

$$\sigma(E)=\sigma(E_0)(E_0/E)[f_{E1}(\eta,\xi)]_E[f_{E1}(\eta,\xi)]_{E_0}^{-1}, \quad (13)$$

and for $E2$ transitions

$$\sigma(E)=\sigma(E_0)[(E-\Delta E')/(E_0-\Delta E')][f_{E2}(\eta,\xi)]_E \times[f_{E2}(\eta,\xi)]_{E_0}^{-1}, \quad (14)$$

where E_0 is the energy at which the curves are normalized, $\Delta E'$ is defined in Eq. (7), and the $f_{E\lambda}$ are tabulated by Alder *et al.*[1]

Since gamma radiation was detected only in the crystal angular acceptance cone centered on an axis perpendicular to the incident beam, it was necessary to make corrections for the angular distributions to be expected for the de-excitation radiations involved. As noted by Alder *et al.*,[1] these angular distributions are given by

$$W_{E\lambda}=1+\sum_{\eta=1}^{\lambda} a_{2n}{}^{E\lambda}A_{2n}{}^{\lambda}P_{2n}(\cos\theta_\gamma), \quad (15)$$

where the $A_{2n}{}^{\lambda}$ are the coefficients in a hypothetical double gamma correlation with the excited state as intermediate and the $a_{2n}{}^{E\lambda}$ are functions of the Coulomb excitation matrix elements and are tabulated by Alder *et al.*[1] Reference to standard tables of Z_1 coefficients[31] shows that for the $\frac{1}{2}+ \xrightarrow{E2} \frac{5}{2}+ \xrightarrow{E2} \frac{1}{2}+$ pure quadrupole transition in F^{19}, $A_2=0.286$ and $A_4=0.381$; for the $\frac{1}{2}+ \xrightarrow{E1} \frac{1}{2}- \xrightarrow{E1} \frac{1}{2}+$ pure dipole transition $A_2=0$ and the gamma angular distribution is isotropic. Since, as noted, the experimental and theoretical cross sections have been normalized, the constant solid-angle factor drops out of the dipole cross section comparisons. In the case of the quadrupole transition the experimentally determined yields have been multiplied by the ratio of the integral of the calculated distribution $W_{E2}(\theta_\gamma)$ over the sphere to that obtained by numerical integration over the effective counter aperture; this correction varies by only 3% for incident He^3 energies from 1.0 to 2.0 Mev.

Curves B and D of Figs. 11 and 12 show these predicted thin-target excitation functions for He^3 and He^4 incident ions. In the case of He^4 bombardments of F^{19} in Fig. 12, the experimental thin-target data of Temmer and Heydenburg[11] have been replotted for comparison. It is clear that there are appreciable discrepancies between the predictions and experiment although qualitative agreement is obtained. Sherr, Li, and Christy,[13] on the other hand, find good agreement between the thin-target predictions and measurements made using a target thickness of ~100 kev of CaF_2 on Al. These discrepancies suggest that multipolarity determination based on excitation curve shapes alone should be treated with some caution.

In order to modify the thin-target curves for com-

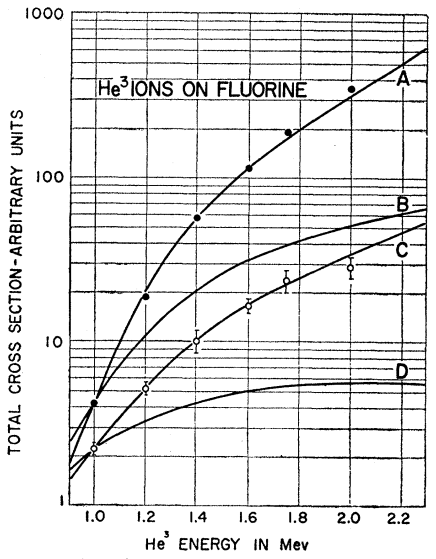

FIG. 11. Comparison of observed and predicted excitation curves for He^3-induced Coulomb excitation of F^{19}. The closed circles are the experimental points for the 197-kev $E2$ transition in F^{19}; the open circles are those for the 110-kev $E1$ transition. Curves B and D are the thin-target and A and C the thick-target predictions, respectively.

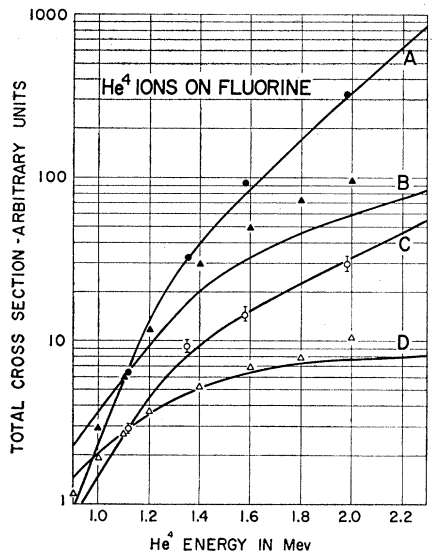

Fig. 12. Comparison of observed and predicted excitation curves for He^4-induced Coulomb excitation of F^{19}. The closed circles are the experimental points for the 197-kev $E2$ transition in F^{19}; the open circles are those for the 110-kev $E1$ transition. Curves B and D are the thin-target and A and C the thick-target predictions, respectively. The closed and open triangles are the thin-target results of reference 11.

parison with the thick-target measurements, use was made of the relation given by Alder *et al.*,[1]

$$Y=\sigma(E_i)\frac{E_iN}{(dE/ds)_{E_i}}\frac{\delta E_\lambda}{E_i}. \tag{16}$$

Here Y is the fraction of the incident particles which produce the Coulomb excitation, N is the density of target atoms, $(dE/ds)_{E_i}$ is the target stopping power at the incident energy, and $\delta E_\lambda/E_i$ (the ratio of the observed yield to that which would result if σ and dE/ds were independent of energy and equal to their values at E_i) has been tabulated by Alder *et al.*[1] on the assumption that $dE/ds\sim E^{-0.55}$ as proposed by Lindhard and Scharff.[32] Again on this assumption,

$$R(E)=\frac{Y(E)}{Y(E_0)}=\frac{\sigma(E)}{\sigma(E_0)}\left(\frac{E}{E_0}\right)^{1.55}\left(\frac{\delta E_\lambda}{E}\right)\left(\frac{\delta E_\lambda}{E_0}\right)^{-1}, \tag{17}$$

and this correction factor $R(E)$ has been used to obtain the thick-target predictions given by curves A and C of Figs. 11 and 12. In these figures curves A and B refer to the 197-kev $E2$ transition and C and D to the 110-kev $E1$ transition. The agreement between experiment and the thick-target predictions is quite satisfactory in the energy range studied; this agreement supports the validity of the $dE/ds\sim E^{-0.55}$ relationship used in obtaining these predictions.

[32] J. Lindhard and M. Scharff, Kgl. Danske Videnskab. Selskab, Mat.-fys. Medd. **27**, No. 15 (1953).

Cross-Section Ratios

From Eq. (1), for electric dipole transitions the predicted cross section ratio, ignoring range correction, is

$$R_{E1}'=\frac{\sigma_{E1}(\mathrm{He}^3)}{\sigma_{E1}(\mathrm{He}^4)}=\frac{m_{\mathrm{He}^3}}{m_{\mathrm{He}^4}}\left(\frac{E_{\mathrm{He}^3}}{E_{\mathrm{He}^4}}\right)^{-1}=0.7535\frac{E_{\mathrm{He}^4}}{E_{\mathrm{He}^3}}. \tag{18}$$

From Fig. 1 it follows that $E_{\mathrm{He}^4}/E_{\mathrm{He}^3}$ is almost exactly constant at 1.127 over the range of energies studied, whence the predicted value for R_{E1}' is 0.849. It should be noted that R_{E1}' is independent both of the target mass and atomic number and of the energy of the transition involved.

Similarly, from Eq. (1), for electric quadrupole transitions in F^{19}

$$R_{E2}'=\frac{\sigma_{E2}(\mathrm{He}^3)}{\sigma_{E2}(\mathrm{He}^4)}=\frac{m_{\mathrm{He}^3}}{m_{\mathrm{He}^4}}\left\{\frac{m_{F^{19}}+m_{\mathrm{He}^4}}{m_{F^{19}}+m_{\mathrm{He}^3}}\right\}^2\left\{\frac{E_{\mathrm{He}^3}-\Delta E_{\mathrm{He}^3}'}{E_{\mathrm{He}^4}-\Delta E_{\mathrm{He}^4}'}\right\}, \tag{19}$$

where $\Delta E'$ is defined by Eq. (7). Inserting mass values and energies involved gives $R_{E2}'=0.72$ in the energy range of interest. In contrast to R_{E1}', this ratio is a function both of the target mass and of the energy of the transition involved.

These calculated thin-target ratios must be corrected however for the fact that at He^3 and He^4 incident energies such that the ξ values are equal, the ranges in the thick targets used are not equal with the He^4 ions having the slightly greater range. Because of this greater range the incident He^4 ions effectively see a greater number of target nuclei and give an apparent yield increase. From the data tabulated by Whaling,[33] and Eq. (6), this correction is constant, within the accuracy of the data, over the range of He^3 and He^4 energies involved, giving a He^3 range equal to 0.895 of that of the corresponding He^4 ions. Applying this correction to the calculated ratios on the assumption of uniform target density gives $R_{E1}=0.895\ R_{E1}'=0.76$ and similarly $R_{E2}=0.64$.

Fluorine-19

Figure 13 shows the ratio data for F^{19} from Table III compared with the ratio calculations as functions of the incident He^3 and corresponding He^4 energies (see Table I). As shown, the electric quadrupole results are in good agreement with the calculations and are independent of the incident energy in the range considered here. The fact that all experimental points lie on the average $\sim 2\%$ below the predictions suggests that the range correction may be in error by this amount.

The electric dipole results are also in good accord

[33] W. Whaling, *Encyclopaedia of Physics*, edited by S. Flügge (Springer-Verlag, Berlin, 1958), Vol. 34.

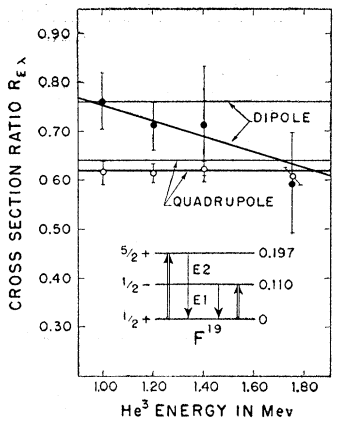

FIG. 13. Coulomb excitation cross-section ratio measurements and calculations for F^{19} as functions of the incident He^3, and corresponding (see Table I) He^4 energies. The inset level diagram shows the transitions studied; the lighter horizontal lines are the theoretical ratio predictions for these transitions.

with theoretical predictions at the lower energies considered. The large errors result from the difficulties involved in extracting the yield of 110-kev radiation as discussed in the previous section. Because of these large errors it is not possible to conclude with certainty that these results represent a significant departure from the theoretical predictions. The results suggest a decrease in the value of R_{E1} with increasing incident energy; such a decrease, if real, might be interpreted as owing to the onset of inelastic excitation of the 0.110-Mev level via nuclear scattering of the alpha particles. Since the number of open channels for the decay of the compound nucleus, once formed, is very much less for alpha than for He^3 bombardments,[17,30] it would be anticipated that the single inelastic scattering channel would become important at lower corresponding He^4 energies with a resultant increase in the 110-kev radiation yield in He^4 bombardments relative to that in He^3 bombardments and an apparent decrease in the Coulomb excitation yield ratio. For either He^3 or He^4 bombardments considered separately, because of the lower excitation energy and angular momentum change involved, an inelastic scattering contribution would be expected to become appreciable for the 110-kev transition at a lower incident ion energy than for the 197-kev transition. It is of interest to note here that Sherr, Li, and Christy[13] as well as Temmer and Heydenburg[11] found no deviation from the Coulomb excitation predictions for the 110-kev excitation function at incident energies below 2.1 Mev although the 1.28-Mev gamma ray from $F^{19}(\alpha,p\gamma)Ne^{22}$ showed appreciable yield and resonance structure at alpha energies above 1.3 Mev, indicating compound nucleus formation.

In considering Coulomb excitation induced by He^3 and He^4 ions the possibility exists of an augmented cross section for incident He^3 ions because of their greater expected polarizability; this would result from the interaction of the induced dipole moment of the incident particle with the target nucleus. In the case of an $E1$ transition this effectively corresponds to the addition of an $E4$ excitation. It was found that in the incident He^3 energy range from 1.0 to 2.0 Mev the contribution to the total cross section from the $E4$ term varies between $\sim 10^{-3}\alpha$ to $3\times 10^{-3}\alpha$ times the normal $E1$ cross section, where α is the He^3 polarizability in units of $(r_{He^3})^3$.[34] Since it would be expected that $\alpha \leqslant 1$ in these units, it follows that this effect is of no consequence in normal Coulomb excitation measurements.

From the spectra of Figs. 6 and 7 it is also possible to deduce an experimental value for the ratios of the 110-kev $E1$ and 197-kev $E2$ excitation cross sections for a given incident particle. These data have been examined in terms of the Nilsson collective model.[3] Simple applications of this model to predict the equilibrium deformations of states in the mass-29 and mass-25 systems have previously been reported.[35,36] When it is similarly applied to F^{19}, the $\frac{1}{2}^-$ state at 110 kev is predicted to have an appreciably larger prolate distortion than the $\frac{1}{2}^+$ ground state or the $\frac{5}{2}^+$ at 197 kev.

Although the eigenfunction normalization used by Nilsson[3] does not permit the calculation of transition widths between states of differing distortion, it was considered of interest to calculate the relative Coulomb excitation cross sections as predicted by the Nilsson model for the $E2$ and $E1$ transitions involving the $\frac{5}{2}^+$ and $\frac{1}{2}^-$ states at 197 and 110 kev on the assumption of a common distortion. From the work of Paul,[37] a prolate distortion $3 \leqslant \eta \leqslant 6$ is indicated, at least for the $\frac{1}{2}^+$ and $\frac{5}{2}^+$ states, depending upon the strength of the spin-orbit term in the potential.

The $\frac{5}{2}^+$ state is found to have $\sim 19\%$ $K=\frac{3}{2}$ and 81% $K=\frac{1}{2}$ configurations,[37] whereas the ground state is of necessity a pure $K=\frac{1}{2}$ state. The 110-kev state is also a pure $K=\frac{1}{2}$ negative-parity state. For values of η in this range and including both single-particle and collective terms in the $E2$ transition,[37] a value of $B(E2)\approx 0.0025$ is obtained in units of $e^2\times 10^{-48}$ cm^4 to be compared to the quoted value of 0.003 as derived from experiment.[2]

Experimentally the ratio of $E1$ to $E2$ cross sections varies from 0.52 to 0.10 for incident He^3 energies between 1.0 and 2.0 Mev; the model predictions for this ratio lie in this range of values for $3 \leqslant \eta \leqslant 3.5$ and $4.5 \leqslant \eta \leqslant 5$. The Nilsson model is thus in accord with the relative observed $E1$ and $E2$ widths although this agreement is perhaps fortuitous since the calculations, of necessity, ignore the probable difference in nuclear shape for the ground and 110-kev states. Clearly it would be desirable to examine other examples of $E1$ excitations to obtain a more stringent test for the ratio technique than is possible in the case of F^{19}.

From the available beta-decay evidence[29] there is the suggestion that the states in Eu^{153} and Gd^{155} at 97.3 and $\sim$100 kev, respectively, have opposite parity

[34] H. McManus (private communication, 1958).
[35] Bromley, Gove, and Litherland, Can. J. Phys. **35**, 1057 (1957).
[36] Litherland, McManus, Paul, Bromley, and Gove, Can. J. Phys. **36**, 378 (1958).
[37] E. B. Paul, Phil. Mag. **15**, 311 (1957).

to that of the ground states and that these should be accessible to $E1$ Coulomb excitation. When they used 6-Mev alpha particles, Heydenburg and Temmer[2] found no evidence for Coulomb excitation of states at these excitations. As noted previously, no others are available in convenient target nuclides. With heavy ions incident, as demonstrated by Newton and Stephens,[6] it should be possible to excite states at excitations up to $\sim$2.5 Mev. A number of possible $E1$ transitions are then amenable to study which are otherwise excluded because their excitation energies are too high to give a measurable excitation cross section. In particular it would be of considerable interest to examine in detail the Coulomb excitation of as many as possible of the odd-parity states in heavy even-even nuclides corresponding to pear-shaped deformations of the nuclear core and octopole nuclear excitations.[38,39]

Sodium-23, Titanium-47, Manganese-55

Table IV lists the ratio measurement results for Na^{23}, Ti^{47}, and Mn^{55} electric quadrupole excitations. The larger error associated with the R_{E2} measurement for Na^{23} reflects the presence of the 0.511-Mev annihilation radiation and the consequent uncertainties in the extraction of the yield of 446-kev radiation from the experimental spectra. The internal consistency in the values obtained for R_{E2} for the $E2$ transitions with this exception is quite good; the average result obtained for the Ti^{47} and Mn^{55} results is 0.63 ± 0.02, in excellent agreement with the calculated value of 0.63 obtained from Eq. (19). The Na^{23} result of 0.55 ± 0.10 agrees within the quoted error with the predicted 0.64.

Parity Mixing

At present there is insufficient information available regarding angular momentum and parity assignments to the low states particularly in heavy nuclides to permit selection of situations where the Coulomb excitation process might provide a probe for determining limits on the intensity of opposite-parity components in the wave functions of the states involved. Transitions of the type 0^+ to 2^- or 0^- to 2^+ would provide the most sensitive test since the cross sections for magnetic excitations coupling the dominant wave function components are in general reduced by at least the factor $(v/c)^2$ over those for the electric excitations coupling to the opposite-parity components. This factor is not in itself sufficient to provide a significant limit compared to those which have been obtained in experiments involving violation of selection rules where limits on the intensity of the opposite-parity components of 10^{-8}–10^{-9} have previously been established[19,40] since for 2-Mev He^4 ions for example $(v/c)^2\sim10^{-3}$.

From the detailed formalism of Eq. (1), however,

$$\frac{\sigma(M2)}{\sigma(E2)}\sim\frac{2\times10^{-7}}{A_1}E^{\frac{1}{2}}(E-\Delta E')^{\frac{1}{2}}\frac{B(M2)}{B(E2)}\frac{f_{M2}(\xi)}{f_{E2}(\xi)}, \quad (20)$$

and for $A_1=1$ for example Alder *et al.* (Fig. II.1a)[1] obtain $\sigma(M2)/\sigma(E2)\sim10^{-5}$ in the range $1\leqslant E\leqslant3$ Mev. It may thus be possible to utilize the Coulomb excitation technique in heavy nuclides where the selection rule methods are more difficult to apply. Heavy ions provide an additional advantage in these measurements because of the A_1^{-1} factor appearing in the ratio.

CONCLUSIONS

Coulomb excitation cross-section ratio measurements on a number of $E2$ transitions have given results which are in quite good agreement with the predictions of the semiclassical theory as corrected for range effects in thick targets. No evidence has been found for nuclear inelastic scattering contributions in the range of bombarding energies considered except in the case of the 110-kev $E1$ transition in F^{19} where this possibility exists. Cross-section ratio measurements on this $E1$ transition are in accord with the theoretical predictions within the accuracy obtainable.

Provided that nuclear inelastic scattering contributions can be excluded it has been demonstrated that the ratio technique provides a method for unambiguous multipolarity determinations.

As expected, the major disadvantages inherent in the use of He^3 ions in Coulomb excitation studies, as compared to He^4 ions, are the higher bremsstahlung cross sections, the intense 0.511-Mev radiation associated with the decay of He^3-induced positron emitters, and the relatively large number of open channels characteristic of He^3-induced reactions, resulting in a high background from high-energy reaction gamma radiation.

Clearly there is considerable interest in the application of the ratio technique to additional dipole transitions; with the energies currently available from heavy-ion accelerators it should be possible to carry out such measurements on transitions to a number of 1^- low-lying states in heavy even-even nuclides.[7] Similarly Coulomb excitation measurements on low-lying 3^- states in these nuclei will provide crucial information on octopole nuclear distortions[39] and the validity of the semiclassical Coulomb excitation formalism for octopole transitions.

ACKNOWLEDGMENTS

We are indebted to Dr. L. G. Elliott, Dr. H. McManus, and Dr. A. E. Litherland for discussions regarding this work, to Miss A. R. Rutledge for computational assistance, and to Mrs. J. S. Merritt and W. Woytowich for radioactive source preparation.

[38] A. Bohr and B. R. Mottelson, Nuclear Phys. 4, 529 (1957), and Nuclear Phys. (to be published).
[39] V. Strutinski, J. Nuclear Energy 4, 523 (1957).
[40] N. Tanner, Phys. Rev. **107**, 1203 (1958).